JMEMS Letters

Thermomechanically Tunable Infrared Metamaterials Using Asymmetric Split-Ring Resonators

Qiugu Wang, Depeng Mao, and Liang Dong

***Abstract*— We demonstrate a nanoelectromechanical systems-based tunable infrared metamaterial formed with an array of Au/Si bilayer split-ring resonators having two asymmetric arms. The wider arm of the resonator is anchored on the substrate, while the thinner one is free to bend in vertical direction by varying temperature. The bending of the thin arm changes the air gap between the two arms, and thus modulates the optical resonance modes of the resonator. The presented tunable metamaterial has an ultra-small footprint size and provides a relatively large optical signal modulation at 3.6-μm wavelength. [2017-0194]**

***Index Terms*— Split-ring resonator, nanoelectromechanical systems (NEMS), thermomechanical, infrared, metamaterials.**

I. Introduction

METAMATERIALS are artificially engineered resonant materials able to manipulate light at a subwavelength scale [1]. They can be designed to strongly interact with the electric and/or magnetic fields of incident electromagnetic (EM) waves, thus enabling many unique properties (e.g., perfect absorption, sub-wavelength focusing, and negative refractive index) [2]. Split-ring resonators are commonly used elements in metamaterials, and can generate a magnetic response that gives a negative permeability. Tunable metamaterials offer the great possibility to actively change their properties through external stimuli [3]. Considerable efforts and progresses have been made towards the realization of high-performance tunable metamaterials with wide operation bandwidths and dynamic EM properties [2]–[21]. Many tunable metamaterials rely on nonlinear materials to alter dielectric properties of the resonators or substrates [5]–[8]. Also, microelectromechanical systems (MEMS) technology has allowed for tuning of the metamaterials by means of adjusting the geometry, structure, and configuration of the lattices [1], [4], [9]–[12]. Active actuation for the MEMS-based metamaterials rely on thermomechanical [1], magnetomechanical [9], electromechanical [12], and optomechanical [13] methods. In addition, flexible substrates [14], [15], liquid metals [2], and stimuli-responsive polymers [16] have been used to realize various tunable metamaterials.

Notably, due to relatively large dimensions of the unit cells and difficulties in achieving sub-wavelength mechanical actuation, most of the reported MEMS metamaterials resonate at terahertz and longer wavelengths. Although several tunable infrared (IR) metamaterials have recently been developed with alternating bendable and non-bendable bridges [17], arrayed pairs of electrically actuated metallic strings [18], and SRRs embedded with nanocantilevers [19], the implementation of mechanically tunable metamaterials in the IR and shorter wavelength regions remains challenging due to the difficulty in efficiently and effectively tuning nanoscale resonators without sacrificing the compactness of the device.

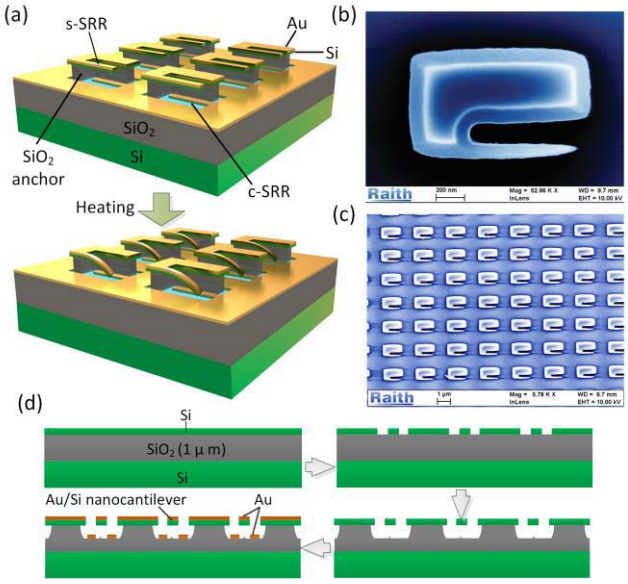

Fig. 1. (a) Schematic of the NEMS-based tunable IR metamaterial before and after heating. (b, c) Scanning electron microscopy (SEM) images of a single s-SRR unit and an array of s-SRR. (d) Fabrication process.

We report a nanoelectromechanical systems (NEMS)-based thermomechanically tunable metamaterial in a mid-IR spectral range. This metamaterial is featured with an array of tunable SRR structures having two asymmetric arms with one fixed and the other thermally bendable. Each SRR has a 1 μm$\times$1.3 μm footprint area and a 170 nm gap distance between the two arms. The relative reflectance change of the metamaterial can reach up to 90% at a resonant wavelength of 3.6 μm.

II. Design and Methods

The tunable IR metamaterial is realized on the top surface of a silicon-on-insulator (SOI) substrate. It consists of an array of metal-dielectric (Au/Si) bilayer solid SRRs (s-SRRs) at the top and another array of complementary SRRs (c-SRRs) at the bottom (Fig. 1a). The Au and Si layers of the s-SRR are 20 nm thick each. One arm of the s-SRR is suspended above the substrate and can bend in the vertical direction, while the other arm is fixed on a SiO_2 anchor.

Manuscript received August 22, 2017; revised September 24, 2017; accepted October 14, 2017. Date of publication October 30, 2017; date of current version November 29, 2017. This work was supported by the U.S. National Science Foundation under Grant ECCS-0954765 and Grant ECCS-1711839. Subject Editor O. Solgaard. *(Corresponding author: Liang Dong.)*

The authors are with the Department of Electrical and Computer Engineering, Iowa State University, Ames, IA 50011 USA, and also with the Microelectronics Research Center, Iowa State University, Ames, IA 50011 USA (e-mail: ldong@iastate.edu).

Color versions of one or more of the figures in this paper are available online at http://ieeexplore.ieee.org.

Digital Object Identifier 10.1109/JMEMS.2017.2764054

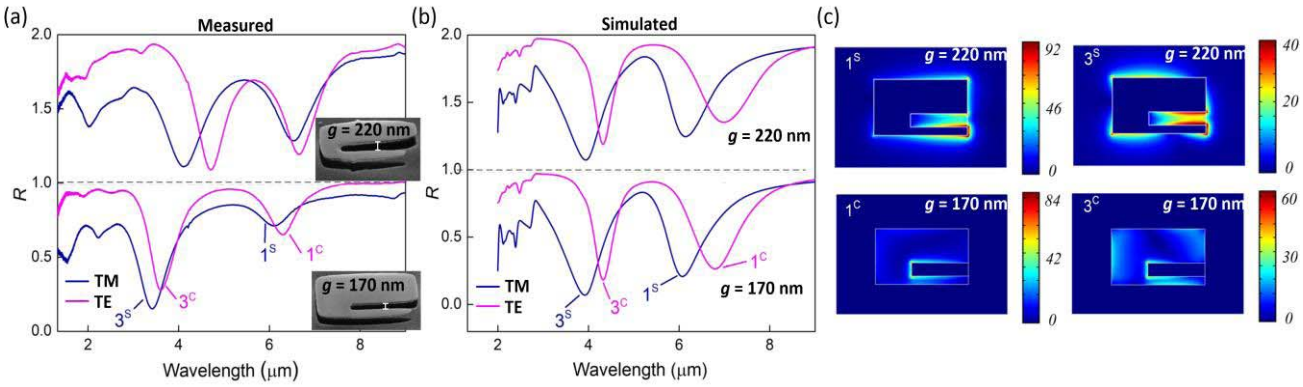

Fig. 2. Measured (a) and simulated (b) reflection spectra of the metamaterials under TM and TE polarizations for two devices with the air gap of 170 nm (bottom) and 220 nm (top). The spectra were measured via the Fourier transform IR (FTIR) microscope system (Hyperion 2000, Bruker) with normal incident light. Insets in (a) show the SEM photos of the unit cells. The spectra for $g = 220$ nm in (a) and (b) are vertically offset by 1 for clarify. (c) Normalized electric field distributions of the modes as denoted in (b). The unit of the electric field strength is V/m.

The thickness of the Au layer is chosen 20 nm so that the bendable Au/Si arm provides a large deflection while the Au layer exhibits a continuous film. A thicker Au layer will lead to a slight redshift of all the resonances [22]. Similarly, to maximize the deflection of the bendable Au/Si arm, the thickness of the Si layer is set at a practically minimal value, i.e., 20 nm. A thinner Si layer will not be able to support itself suspended. The planar distance between the two arms is $g = 170$ nm (Fig. 1b). The SiO_2 anchor is 100 nm thick. The bottom c-SRR has an inverse shape to the top s-SRR as an aperture in the 20 nm-thick Au layer at the substrate surface. Depending on the polarization direction of incident light, different eigenmodes of the s-SRR or c-SRR can be excited. As the metamaterial is heated up, the thin arm of the s-SRR will bend down towards the c-SRR due to a difference in thermal expansion coefficient between Au and Si. This, in turn, will alter the air gap between the two arms (Fig. 1a), thus tuning the optical properties of the eigenmodes of the s-SRR or c-SRR.

Fabrication of the tunable IR metamaterial (Fig. 1c) starts with a bare SOI substrate composed of a 340 nm-thick top Si layer, a 1 μm-thick buried oxide, and a 580 μm-thick handling substrate (Fig. 1d). First, the top Si layer is thinned down to 50 nm thickness by wet oxidation of Si for 59 min. After the removal of oxide using a buffered oxide etcher (BOE), dry oxidization is conducted for another 34 min to precisely reduce the thickness to 20 nm. The obtained Si thickness is 20 nm with a uniformity variation of 5% over a 3-inch wafer. Subsequently, s-SRRs are patterned in the top Si via e-beam lithography and subsequent reactive ion etching of Si. Next, the thinner arm of the SRR is released from the substrate by immersing the device into the BOE solution for 2 min to etch $\sim$100 nm-thick SiO_2 from underneath the thinner arm. For the wider arm, only the edge part of the SiO_2 anchor is etched. Finally, a 20 nm-thick Au film is evaporated to form the s-SRRs. During evaporation, the s-SRRs serve as a shadow mask, allowing the formation of the c-SRRs in the Au layer on the substrate surface.

III. Results and Discussion

Fig. 2a shows the measured optical reflection spectra of the fabricated IR metamaterial under transverse magnetic (TM) and transverse electric (TE) polarizations at room temperature ($T_o = 21°C$). Conspicuous resonance dips are observed at different wavelengths. In general, when the incident field is polarized along the parallel (TM) or perpendicular (TE) directions to the gap of s-SRR, odd or even eigenmodes will be excited for s-SRRs. In contrast, even or odd eigenmodes of c-SRRs will be excited by the TM or TE field, respectively. Specifically, in the case that the s-SRR has a 170 nm-wide gap between the two arms (lower panel of Fig. 2a), there appear two odd modes as reflection dips under the TM polarization. We mark the resonance modes with '1^S' at a wavelength of 6 μm, and '3^S' at 3.4 μm in the spectrum, where the superscripts 'S' denote s-SRR modes. Under the TE polarization, two odd-order c-SRR modes, i.e., 1^C at 6.1 μm and 3^C at 3.6 μm, are excited, where the superscripts 'C' denote c-SRR modes. To identify the order of these modes, the corresponding electric field distributions are plotted (Fig. 2c). For the 1^S mode, only one electric field node is observed while the 3^S mode exhibits three nodes. Because the c-SRR is inversed relatively to the s-SRR, the reflection spectrum of the c-SRR for the TE polarization appears similar to that of the s-SRR for the TM polarization, according to the Babinet principle [19]. The discrepancies between the simulated and experimental results (Fig. 2a-b) may be caused by the inevitable errors of the geometric parameters used in the model, compared to the real values.

To investigate how the air gap of the s-SRR influences the s-SRR and c-SRR modes, we increased the gap size from 170 nm to 220 nm (upper panel of Fig. 2a). With increasing the value of g, all the resonance modes exhibit slight redshifts, and the resonances at shorter wavelengths show greater shifts. This result indicates that altering the air gap between the two arms of the s-SRR can tune the optical properties of the metamaterial.

Fig. 3a and 3b (top panels) shows that with increasing temperature, all the reflectance dips of the metamaterial ($g = 170$ nm) consistently exhibit positive changes in intensity, resulting from the bending of the thin arm of the s-SRR. To highlight the temperature induced variations of reflection intensity, we plot relative reflectance changes at different temperatures: $\Delta R/R_o = (R-R_o)/R_o$, where R and R_o represent the reflection intensity at applied temperature T and room temperature T_o, respectively. The obtained spectra of $\Delta R/R_o$ (bottom panels of Fig. 3a-b) exhibit peak-like features. Both the 3^S TM mode and the 3^C TE mode exhibit relatively large changes in reflectance with an increase in temperature. Specifically, when the temperature rise increases from $\Delta T = 0$ to 173 °C, the reflectance at the 3^S mode increases from 11.9% to 20.5% (top panel of Fig. 3a), which corresponds to $\Delta R/R_o = 77\%$ (bottom panel of Fig. 3a). Accordingly, $\Delta R/R_o$ at the 3^C mode reaches 91% for $\Delta T = 173$ °C. In contrast, the lower order modes present much less changes in reflectance, which are almost zero for the 1^S mode, and 11.8% for the 1^C mode. With decreasing gap size g, the 1^S or 1^C mode may become weakly excited

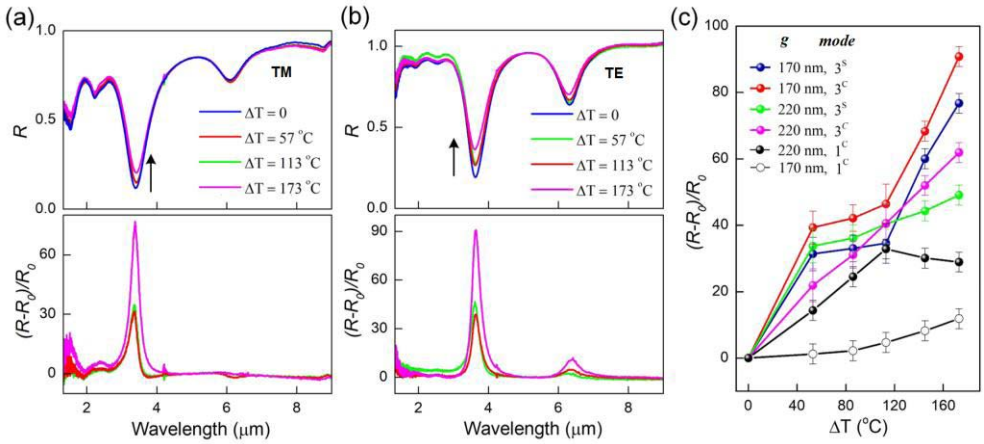

Fig. 3. (a, b) Measured reflection spectra (top panels) of the metamaterial ($g = 170$ nm) under TM (a) and TE (b) polarizations. The bottom panels show the corresponding $\Delta R/R_0$ spectra at different temperature rises ΔT above the room temperature (21°C). The device temperature was changed by a mini heater emplaced below the metamaterial. Temperature was monitored by a thermocouple. (c) Summary of the values of $\Delta R/R_0$ as a function of ΔT for different resonances.

due to the increased radiation damping within the gap, thus showing a reduced sensitivity to the cantilever deflection. In contrast, as the value of g increases to 220 nm, the value of $\Delta R/R_0$ for the 1^C mode significantly decreases, exhibiting the maximal change of 33% at $\Delta T = 173$ °C, as shown in Fig. 3c.

The temperature coefficient for the refractive index of Au or n_{Au} was $dn_r/dT = 3.408 \times 10^{-4}$ K^{-1} and $dn_i/dT = -1.381 \times 10^{-4}$ K^{-1}, where n_r and n_i are the real and imaginary part of n_{Au} [23]. At room temperature (300 K), $n_{Au} = 0.1313+3.6548i$. For $\Delta T = +173$ K, the real part of Au permittivity has almost no change while the imaginary part increases from 0.96 to 1.38, indicating an energy loss by Au and thus a trend to reduce the reflectance of Au. Since Fig. 3a-b show that increasing temperature results in a rise in reflectance of the metamaterial, one can conclude that the cantilever deflection induced increase in reflectance is larger than the temperature induced reflectance reduction.

Fig. 3c summarizes the modulation of reflection intensity at the resonance modes for the metamaterials with $g = 170$ nm and 220 nm. As the temperature rise ΔT increases, the changes in reflectance at the resonance modes for the smaller-gap device become more significant than those for the larger-gap one.

IV. Conclusions

We demonstrated a tunable IR metamaterial with a small footprint size by thermal actuation of asymmetric s-SRRs. This metamaterial has a small footprint size and provides a relative reflectance change of up to 90% at 3.6 μm wavelength.

References

[1] H. Tao, A. C. Strikwerda, K. Fan, W. J. Padilla, X. Zhang, and R. D. Averitt, "Reconfigurable terahertz metamaterials," *Phys. Rev. Lett.*, vol. 103, no. 14, p. 147401, Oct. 2009.

[2] P. Liu *et al.*, "Tunable meta-atom using liquid metal embedded in stretchable polymer," *J. Appl. Phys.*, vol. 118, no. 1, p. 014504, Jul. 2015.

[3] P. Pitchappa, C. P. Ho, Y. Qian, L. Dhakar, N. Singh, and C. Lee, "Microelectromechanically tunable multiband metamaterial with preserved isotropy," *Sci. Rep.*, vol. 5, Jun. 2015, Art. no. 11678.

[4] A. Q. Liu, W. M. Zhu, D. P. Tsai, and N. I. Zheludev, "Micromachined tunable metamaterials: A review," *J. Opt.*, vol. 26, no. 11, p. 114009, Sep. 2012.

[5] S. Xiao, U. K. Chettiar, A. V. Kildishev, V. Drachev, I. C. Khoo, and V. M. Shalaev, "Tunable magnetic response of metamaterials," *Appl. Phys. Lett.*, vol. 95, no. 3, p. 033115, Jul. 2009.

[6] Q. Wang, W. Han, P. Liu, and L. Dong, "Electrically tunable quasi-3-D mushroom plasmonic crystal," *J. Lightw. Technol.*, vol. 34, no. 9, pp. 2175–2181, May 1, 2016.

[7] M. Seo *et al.*, "Active terahertz nanoantennas based on VO_2 phase transition," *Nano Lett.*, vol. 10, no. 6, pp. 2064–2068, Jun. 2010.

[8] Q. Wang *et al.*, "Optically reconfigurable metasurfaces and photonic devices based on phase change materials," *Nature Photon.*, vol. 10, no. 1, pp. 60–65, Jan. 2016.

[9] M. Lapine, I. V. Shadrivov, D. A. Powell, and Y. S. Kivshar, "Magnetoelastic metamaterials," *Nature Mater.*, vol. 11, no. 1, pp. 30–33, Jan. 2012.

[10] W. M. Zhu *et al.*, "Polarization dependent state to polarization independent state change in THz metamaterials," *Appl. Phys. Lett.*, vol. 99, no. 22, p. 221102, Nov. 2011.

[11] W. M. Zhu *et al.*, "Switchable magnetic metamaterials using micromachining processes," *Adv. Mat.*, vol. 15, pp. 1792–1796, Feb. 2011.

[12] F. Ma, Y.-S. Lin, X. Zhang, and C. Lee, "Tunable multiband terahertz metamaterials using a reconfigurable electric split-ring resonator array," *Light Sci. Appl.*, vol. 3, no. 5, p. e171, May 2014.

[13] A. Karvounis, J.-Y. Ou, W. Wu, K. F. MacDonald, and N. I. Zheludev, "Nano-optomechanical nonlinear dielectric metamaterials," *Appl. Phys. Lett.*, vol. 107, no. 19, p. 191110, Nov. 2015.

[14] H. Tao *et al.*, "Terahertz metamaterials on free-standing highly-flexible polyimide substrates," *J. Phys. D, Appl. Phys.*, vol. 41, no. 23, p. 232004, Dec. 2008.

[15] I. E. Khodasevych *et al.*, "Elastomeric silicone substrates for terahertz fishnet metamaterials," *Appl. Phys. Lett.*, vol. 100, no. 6, p. 061101, Feb. 2012.

[16] Q. Wang *et al.*, "Tunable optical nanoantennas incorporating bowtie nanoantenna arrays with stimuli-responsive polymer," *Sci. Rep.*, vol. 5, Dec. 2015, Art. no. 18567.

[17] J. Y. Ou, E. Plum, L. Zhang, and N. I. Zheludev, "Reconfigurable photonic metamaterials," *Nano Lett.*, vol. 11, pp. 2142–2144, Apr. 2011.

[18] J. Y. Ou, E. Plum, L. Zhang, and N. I. Zheludev, "An electromechanically reconfigurable plasmonic metamaterial operating in the near-infrared," *Nature Nanotechnol.*, vol. 8, pp. 252–255, Apr. 2013.

[19] Q. Wang, D. Mao, P. Liu, T. Koschny, C. M. Soukoulis, and L. Dong, "NEMS-based infrared metamaterial via tuning nanocantilevers within complementary split ring resonators," *J. Microelectromech. Syst.*, to be published. [Online]. Available: http://ieeexplore.ieee.org/document/8036411/, doi: 10.1109/JMEMS.2017.2746688.

[20] X. Liu and W. J. Padilla, "Dynamic manipulation of infrared radiation with MEMS metamaterials," *Adv. Opt. Mater.*, vol. 1, pp. 559–562, Aug. 2013.

[21] W. M. Zhu *et al.*, "A MEMS tunable metamaterial filter," in *Proc. IEEE 23rd Int. Conf. Micro Elect. Mech. Syst. (MEMS)*, Jan. 2010, pp. 196–199.

[22] L. M. Pulido-Mancera, J. D. Baena, and J. L. A. Quijano, "Thickness effects on the resonance of metasurfaces made of SRRs and C-SRRs," in *Proc. Antennas Propag. Soc. Int. Symp. (APSURSI)*, Jul. 2013, pp. 314–315.

[23] S. K. Ozdemir and G. Turhan-Sayan, "Temperature effects on surface plasmon resonance: Design considerations for an optical temperature sensor," *J. Lightw. Technol.*, vol. 21, pp. 805–814, Mar. 2003.